American Mineralogist, Volume 110, pages 748–756, 2025

# Mechanistic understanding of the dehydroxylation reaction of smectites: Insights from reactive force field (ReaxFF) molecular dynamics simulation

Pengyuan Gao[1,2], Yingchun Zhang[1,2], Xiandong Liu[1,2,*], and Xiancai Lu[1,2]

[1]State Key Laboratory of Critical Earth Material Cycling and Mineral Deposits, School of Earth Sciences and Engineering, Nanjing University, Nanjing, Jiangsu 210023, P.R. China
[2]Frontiers Science Center for Critical Earth Material Cycling, Nanjing University, Nanjing, Jiangsu 210023, P.R. China

## Abstract

Smectite, a major barrier material for contaminants in Earth's critical zone, is a layered aluminosilicate mineral with *cis*-vacant (*cv*) and *trans*-vacant (*tv*) configurations. High-temperature transformations of smectite are directly related to smectite's thermal reactions. However, the precise thermal reaction mechanisms and thermally induced structural transitions of *cv* and *tv* smectite remain debated. In this study, we systematically investigated the mechanism of thermal reactions of *cv* and *tv* smectite models using reactive force field (ReaxFF) molecular dynamics. We explored the deprotonation and the intralayer dehydration steps of *cv* and *tv* smectites at 700 and 900 K. The results revealed that the dehydroxylation reaction of *cv* smectite exhibited more difficulty than *tv* smectite at 700 K, while demonstrating less difficulty at 900 K. Furthermore, it was found that the dehydroxylated *cv* and *tv* smectites evolved to a consistent structure spontaneously. Our findings further confirmed that *cv* smectite has a higher dehydroxylation temperature than *tv* smectite and thus provided a theoretical basis for distinguishing *cv* and *tv* smectites using thermogravimetric analysis (TGA). Moreover, we gathered TGA data of smectites from different regions, confirming that montmorillonites have a *cv* structure and almost all smectites from China (over 11 provinces) are *cv*. This study provides a molecular-level understanding of the thermal reaction mechanisms of smectites and a physical basis for further study and application of smectites.

**Keywords:** Reactive force field molecular dynamics, metadynamics, smectite, *cis*-vacant, *trans*-vacant, thermal reactions

## Introduction

In recent years, there has been a significant surge of scientific interest in investigating the properties of smectites due to their low permeability, high-adsorption capacity, and swelling properties (Bergaya and Lagaly 2006). These characteristics allow them to play key roles in various important applications, such as nuclear waste geologic repositories and natural contaminant barriers, as well as environmental remediation and material development (Tournassat et al. 2015; Guimarães and Bobos 2021; Worasith and Goodman 2023).

Smectites undergo spontaneous modification and transformation as environmental conditions change (Bergaya and Lagaly 2006). In particular, thermal treatment induces alterations in several properties of smectites, encompassing adsorption capacities, swelling behavior, thermal conductivity, and mechanical strength (Heller-Kallai 2013). These changes are associated with high-temperature transformations influenced by thermal reactions (Derkowski and Kuligiewicz 2022). Therefore, a comprehensive understanding of the thermal behavior of smectites is crucial for elucidating their potential applications and limitations in both natural and engineering contexts.

Smectite is a family of clay minerals, which consists of two corner-sharing silicate tetrahedral sheets and one central edge-sharing alumina octahedral sheet (TOT), exhibiting a 2:1 type layer structure (Tournassat et al. 2015). In the TOT layer, the octahedral sites are surrounded by four O atoms and two hydroxyl (OH) groups. According to the position of OH groups, i.e., opposite and adjacent corners, the octahedral sites are distinguished as *trans*-octahedra and *cis*-octahedra. A third of the octahedral sites are vacant. Hence, the TOT layers can be divided into *cis*-vacant (*cv*) exhibiting *C*2 symmetry and *trans*-vacant (*tv*) structures exhibiting *C*2/*m* symmetry (Fig. 1a) (Tsipursky and Drits 1984; Brigatti et al. 2006). The latest research revealed disparities in surface reactivity between the two structures, i.e., the water adsorbed in the interlayer of *cv* structures exhibits stronger ordering and lower density than in *tv* structures (Subramanian et al. 2020). In addition, our recent investigations on smectite surface acidity identified that the edge surfaces of the *cv* structure exhibit positive or negative charges depending on the crystal plane orientation when pH values are below 7, while the *tv* structure consistently displays a negative charge in the common pH range (Gao et al. 2023, 2024). These distinctions can affect the smectite adsorption properties of various pollutants such as metals or metalloids. However, despite the extensive utilization of smectites in various fields, the classification of *cv*/*tv* structures in China remains unresolved.

X-ray diffraction (XRD) techniques, transmission electron microscopy (TEM), and scanning electron microscopy (SEM) and advanced spectroscopic techniques can be used to directly identify and discern structural differences between *cv* and *tv* smectites (Manceau et al. 2000; Subramanian et al. 2020; Orucoglu et al. 2022). However, spectroscopic measurements

* Corresponding author E-mail: xiandongliu@nju.edu.cn https://orcid.org/0000-0003-3966-3998

0003-004X/25/0005–748$05.00/DOI: https://doi.org/10.2138/am-2024-9445

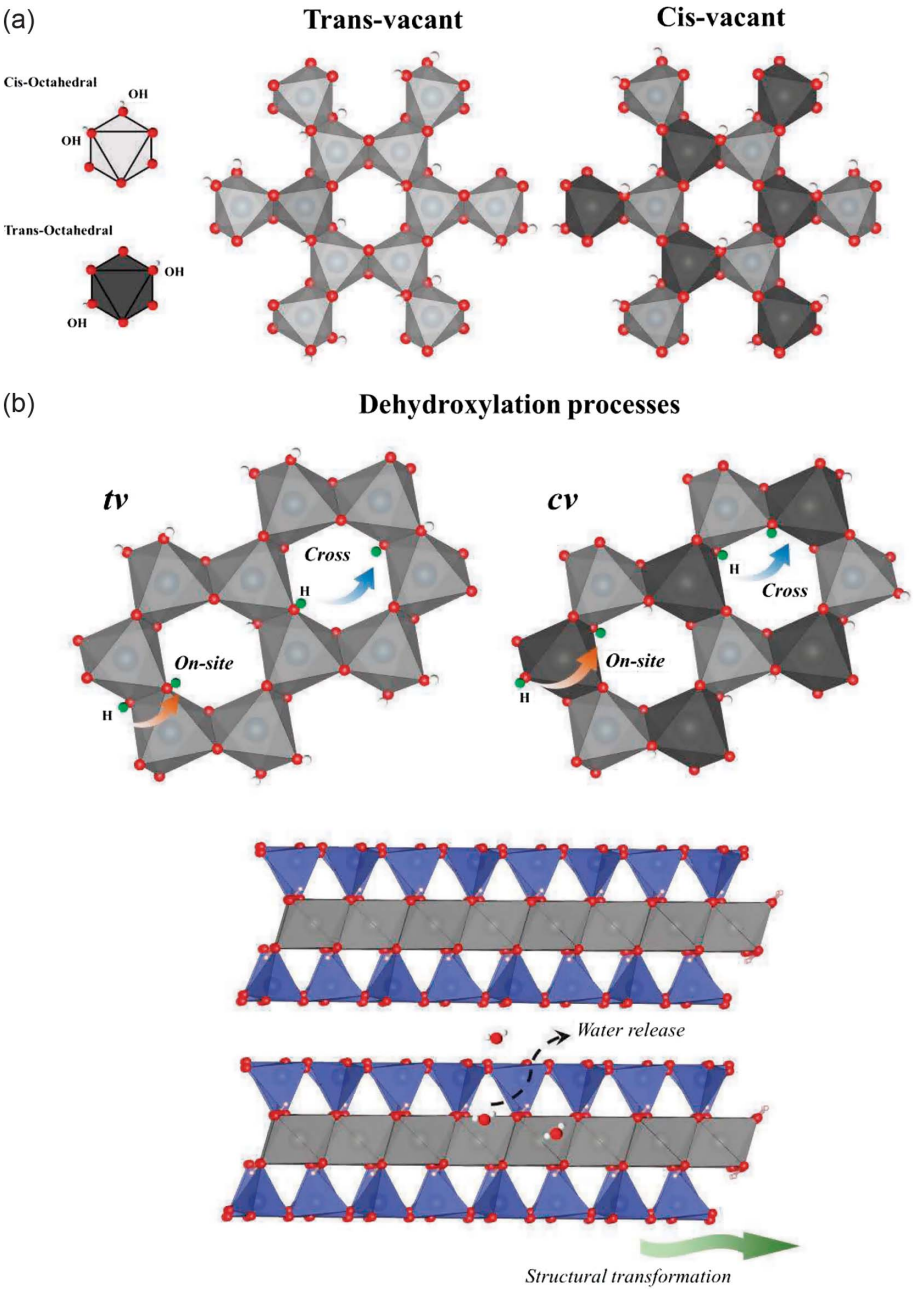


**Figure 1.** Octahedral sheet with *tv* and *cv* configurations (**a**), dehydroxylation processes of deprotonation reactions with cross and on-site mechanism for *cv* and *tv* models, and schematic of the intralayer dehydration process with structural transformation (**b**). (Color online.)

demand high purity, crystallinity, and stability of the smectite samples, which makes it challenging to achieve successful observations. Thermogravimetric analysis (TGA) is the earliest instrumental method applied to clay minerals and serves as the original method for classifying smectites (Derkowski and Kuligiewicz 2022). The distinction between *cv* and *tv* smectites can typically be made based on the boundary temperature of thermal reactions (Lantenois et al. 2008; Emmerich et al. 2009; Derkowski and Kuligiewicz 2022). Therefore, comprehending the thermal properties of *cv* and *tv* structures is crucial to understanding the thermal behavior of smectite under diverse conditions, thereby playing a pivotal role in elucidating the fundamental characteristics of smectite. Nevertheless, there are no investigations on the distinction of structural types of smectites in China through relevant techniques.

The thermal reaction of smectite is observed to occur with increasing temperature, involving interlayer dehydration and intralayer dehydroxylation reactions, as well as crystallization of new phases (Heller-Kallai 2013). Dehydroxylation reactions include deprotonation and dehydration steps and subsequent structural transformations (Fig. 1b). Deprotonation and dehydration reactions in the intralayer occur over a broad temperature range, about 300–800 °C (Derkowski et al. 2012), which is ascribed to differences in the local structural environments of

the hydroxyl (OH) groups (Drits et al. 1995; Molina-Montes et al. 2008a). For instance, it was proposed that the temperature of dehydroxylation for the *tv* smectite (around 300–600 °C) is lower than *cv* type (above 600 °C) (Derkowski and Kuligiewicz 2022). Drits et al. (1995) assigned the difference to the probability of proton transfer in the two structures and the additional Al cation migration step in *cv* smectite, but the specific mechanisms involved remain unclear. Besides, XRD results revealed that *cv* smectites undergo successive dehydroxylation-rehydroxylation reactions and transform into a *tv* structure, which implied distortions in the dehydration structures (Drits et al. 1995). Magic angle spinning nuclear magnetic resonance (MAS NMR) spectroscopic and infrared spectroscopy (IR) analysis showed that alumina octahedra are transformed into a distorted trigonal-bipyramidal five-coordinated structures upon dehydroxylation, whereas silicate tetrahedra were also distorted but still intact (Fitzgerald et al. 1996; Wang et al. 2002). Although these spectroscopy methods were used to trace structural changes during high-temperature transformations of smectite, the transformations still pose challenges to the experimental study of the thermal reaction mechanism due to low crystallinity, disorder, and dispersion properties (Geiger 2008).

Theoretical calculations provide new methods for thermal reaction mechanism investigations. Density functional theory (DFT) calculations were applied to study the energy barrier of the deprotonation process, and various reaction mechanisms have been proposed (Stackhouse et al. 2004; Molina-Montes et al. 2008a). However, since the static calculation is unable to take into account the effect of temperature, it is difficult to provide a reasonable explanation for experimental observations. In recent decades, molecular dynamics (MD) simulations were also employed to investigate the deprotonation reaction in *tv* smectite models, elucidating both on-site (proton migrates in one octahedron) and cross (proton migrates in the vacant) mechanisms (Fig. 1b) as reactive pathways through metadynamics (Molina-Montes et al. 2008b, 2008c, 2010, 2013; Muñoz-Santiburcio et al. 2012, 2016). The energy barrier of the deprotonation step at 900 K suggested that the cross mechanism is favored over the on-site mechanism (38.3 vs. 49.9 kcal/mol) (Molina-Montes et al. 2008b). In addition, the energy barrier of the intralayer dehydration step (around 19–24 kcal/mol) is lower than the deprotonation step (Molina-Montes et al. 2013). After intralayer dehydration, five-coordinated Al sites are further found in the TOT layers (Molina-Montes et al. 2010). Theoretical studies mentioned above were all based on the assumption that *cv* smectite is converted to *tv* smectite during thermal reactions (Drits et al. 1995), and thus only the *tv* smectite model was investigated. However, to the best of our knowledge, the related conversion and thermal reaction mechanisms of *cv* smectite have not been reported.

Molecular simulation methods can be categorized into quantum mechanical and classical mechanical based on the calculation methods (Frenkel and Smit 2002). Quantum mechanical methods directly solve the electronic structures of the system, which can provide accurate results but are computationally intensive and only suitable for small systems with limited simulation timescales (~tens of picoseconds). Classical mechanical methods employ empirical force fields to calculate the potential energy of a system, which enables simulations at much larger spatial and temporal scales. However, the force fields widely used in geochemical modeling are not capable of describing chemical reaction processes, e.g., CLAYFF, INTERFACE, etc. (Heinz et al. 2013; Cygan et al. 2021). The Reactive force field (ReaxFF) method has demonstrated its efficacy in simulating chemical reactions across a wide range of elements and diverse bonding characteristics (van Duin et al. 2001; Senftle et al. 2016). Because the force field is bond-order based, ReaxFF MD can easily reach the timescale of hundreds of picoseconds. Recently, our group has developed a ReaxFF force field model containing several of the most common elements in earth materials under high *T-P* conditions (Zhang et al. 2024). The force field has been systematically tested and proven capable of accurately describing the properties of various systems involving silicate minerals, including solids, melts, fluids, interfaces, etc. As a result, it can be effectively utilized for modeling the thermal reactions of layered silicates.

In this study, we carried out ReaxFF molecular dynamics modeling to systematically investigate the deprotonation reaction within the cross mechanism of *cv* and *tv* smectite models, as well as intralayer dehydration reactions and thermal transformations at 700 and 900 K at the atomic level. The free energy surfaces (FES) and energy barriers of the thermal reactions were obtained using ReaxFF-based metadynamics, which provided a basis for applying the criteria to determine the *cv*/*tv* transition using dehydroxylation temperature proposed by Drits et al. (1995). Then, TGA data were used to categorize the structural types (*cv* or *tv* models) of smectite samples from different geographic regions. This study provides a fundamental understanding of thermal reaction mechanisms for *cv* and *tv* smectites, offering valuable information for future applications of smectites in various fields.

## Methodology

### Models

A 3 × 2 × 2 periodic supercell of 15.54 × 17.94 × 20.10 Å was constructed for the *cis*-vacant (*cv*) and *trans*-vacant (*tv*) structures (as shown in Fig. 2) by using the *cv* and *tv* unit cell, respectively (Online Materials[1] Fig. S1). The model size was examined using a larger supercell, and the similar results suggest that the model is sufficient (Online Materials[1] Fig. S2). Because the Mg content is much lower than Al in the octahedral sheets of smectites, dehydroxylation reactions primarily occur at aluminum sites. Moreover, the interlayer cations generated by isomorphic substitution are not the most important factor in the dehydroxylation process (Koster van Gross and Guggenheum 1989). The presence of interlayer water may impact the dehydroxylation reaction energy but has little effect on the free energy barrier. Therefore, only electrically neutral structures without interlayer water were taken into account in the simulations. The mineral formulas of the unit cells of our *cv* and *tv* smectite models were $Al_4Si_8O_{20}(OH)_4$. For the dehydrated model, half of the hydroxyl groups and the corresponding number of protons were removed compared to the initial models (Online Materials[1] Fig. S3).

### ReaxFF molecular dynamics

The ReaxFF molecular dynamic simulations were performed using reax/c (Aktulga et al. 2012) in the LAMMPS package (Plimpton 1995). The ReaxFF force field developed by our group for Si/Al/O/H/Na/K interactions was used to perform reactive molecular modeling (Zhang et al. 2024). For MD, the simulations were performed in a canonical (NVT) ensemble employing Nóse-Hoover thermostats with a time step of 0.25 fs at temperatures of 700 and 900 K (Martyna et al. 1992). The conjugate gradient (CG) algorithm was used for the structural relaxation calculations with a convergence criterion of $10^{-6}$ kcal/mol.

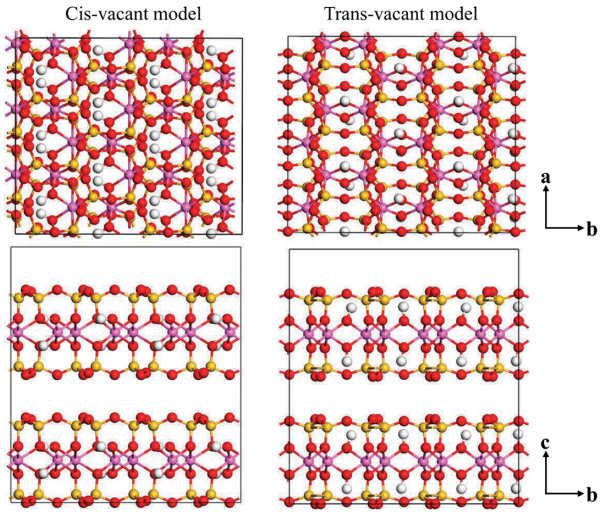


**Figure 2.** The supercell of *cv* and *tv* models. Pink, yellow, red, and white spheres represent Al, Si, O, and H atoms, respectively. (Color online.)

## Free energy calculations

The high-temperature transformations of smectites are primarily governed by dehydroxylation reactions (including deprotonation and dehydration steps) below the critical temperature of amorphization. The thermodynamics of these reactions are associated with physical-chemical properties, which are dependent on specific *cv*/*tv* structure types. The metadynamics method implemented in the PLUMED2 package was used to quantitatively access the free energy surface (FES) of the thermal reactions subjected to the specific collective variables (CVs) for *cv* and *tv* smectites (Laio and Parrinello 2002; Tribello et al. 2014). Considering the lower dehydroxylation energy barrier of the cross mechanism in the *tv* model (Molina-Montes et al. 2008b) and the opposite position of OH in the aluminum octahedron in the *cv* model (Fig. 1), it can be inferred that the cross mechanism is more feasible. The deprotonation reaction with the cross mechanism involves a proton (H) migration from one O atom (denoted as $O_i$) to another O atom across the octahedral vacancy (denoted as $O_{cr}$) (Fig. 3). The distance H-$O_i$ (CV1) and H-$O_{cr}$ (CV2) were employed as CVs, consistent with previous studies (Molina-Montes et al. 2008b; Muñoz-Santiburcio et al. 2012). For the dehydration step, the distance of the mass center of apical O atom ($O_{ap1}$ and $O_{ap2}$) from $O_i$ in the z-direction (dz) served as CV1 to ensure the release of water within the layer (Fig. 3). Meanwhile, the distance component in the xy-plane (dxy) was used as CV2 to observe the possible migration process of water in the interlayer. Additionally, the H-$O_i$ bonds of the intralayer water molecule (Fig. 3) were constrained to prevent proton dissociation in the simulations, thereby making the dehydration step possible. The Gaussian widths for CVs were set to 0.1 Å with a height of 0.2 kcal/mol, which were added every 25 fs in the metadynamics runs.

## Thermogravimetric analysis

Two smectite samples from China (Gaomiaozi) and the U.S.A. (STx) were purified by using the sedimentation method (Tong et al. 2023). STx-smectite was obtained from the source clays repository of the Clay Minerals Society (CMS). TGA of the samples was performed in the range 20~830 °C using a Linseis PT 1600 thermal analyzer with a dry $N_2$ flow rate of 50 mL/min and a constant heating rate of 5 °C/min.

# Results and Discussion

## Mechanism of thermal transformation

**Deprotonation reaction.** The deprotonation process of the *cv*/*tv* models involves the continuous breaking and formation of H-$O_i$ bonds (Online Materials[1] Fig. S4), followed by subsequent protonation/deprotonation of the surrounding apical O atoms ($O_{ap}$ in Online Materials[1] Fig. S5), which was also found in previous studies (Muñoz-Santiburcio et al. 2012). The configuration of the proton coordinated to the $O_{ap}$ is a reaction intermediate accompanied by local deformation (Online Materials[1] Fig. S6). The average Si-$O_{ap}$ distance was 1.65 Å, in the typical range for the silanol group, while the Al-$O_{ap}$ distance was ~2.43 Å, larger than the Al-O distance in the alumina octahedra (around 2.00 Å). The results indicated the formation of silanol groups in the dehydroxylation process, which is consistent with experimental observations (Vantelon et al. 2001). The hydrated products of *cv* and *tv* smectites with water molecules are displayed in Online Materials[1] Figure S7. Both structures exhibit only slight tetrahedral and octahedral distortion, indicating that the deprotonation step does not cause significant structural changes.

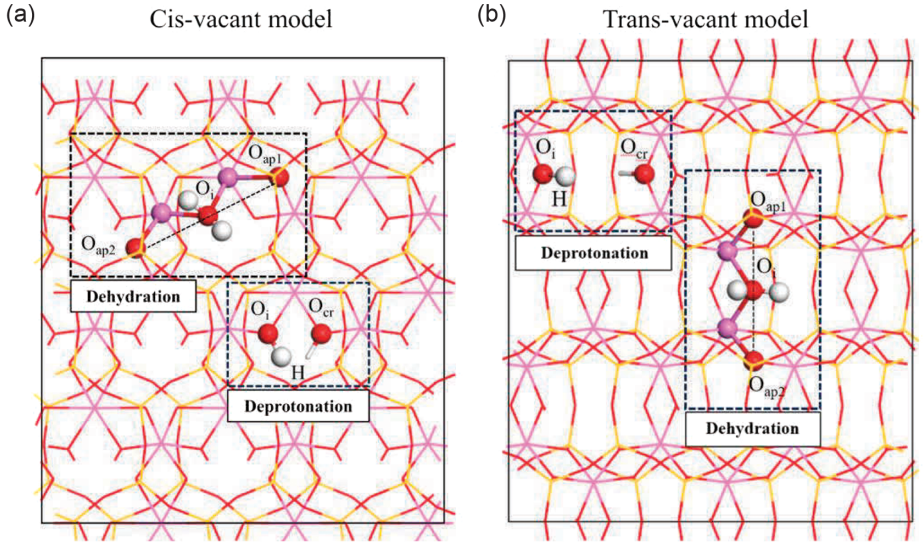


**Figure 3.** The relevant atom labels employed in the *cv* and *tv* smectite models: *cis*-vacant (**a**) and *trans*-vacant (**b**). (Color online.)

The 2D-FES reconstructed from the deprotonation reaction metadynamics simulation at 700 and 900 K are shown in Online Materials[1] Figure S8, as well as the minimum free energy path projected on CV1 (Fig. 4). The evolution of the CVs is shown in Online Materials[1] Figure S4, suggesting the deprotonation reactions were successfully observed. From the free energy profile with respect to CV1, we estimated the deprotonation free energy barrier through the cross mechanism to be 38.6 and 36.5 kcal/mol for *cv* and *tv* smectites at 700 K, respectively, which indicated that the deprotonation is more difficult to occur in *cv* than in *tv*. At 900 K, FESs revealed that the free energy barriers of *cv* and *tv* smectites were 32.3 and 35.2 kcal/mol, respectively (Fig. 4). The values obtained for the *tv* model are in accordance with the range of previous first-principles molecular dynamics simulations (153.1–208.8 kJ/mol for *tv* model) (Molina-Montes et al. 2008b). The results demonstrated that an increase in temperature causes a decrease in free energy barriers, similar to previous studies (Molina-Montes et al. 2008b; Muñoz-Santiburcio et al. 2012). In particular, the free energy barriers of *cv* smectites exhibited a more significant decrease (38.6 vs. 32.3 kcal/mol) with increasing temperature, in contrast to *tv* smectites (36.5 vs. 35.2 kcal/mol). This implied that the deprotonation reaction of *cv* smectite is more sensitive to temperature than the *tv*, and at the temperature of 900 K, the deprotonation reaction is even more feasible.

**Intralayer dehydration reaction.** We then investigated the release of the formed water to the interlayer space of *cv* and *tv* smectites at 700 and 900 K, respectively (Fig. 5; Online Materials[1] Fig. S9). With the evolutions of CVs in metadynamics (Online Materials[1] Fig. S4), we successfully observed the release of water molecules.

In the metadynamics trajectory, the release of water molecules from the structural layer to the interlayer space occurs within a few tens of picoseconds. Subsequently, there is a migration of the water molecule occurring in the interlayer (Online Materials[1] Fig. S4). The reconstructed 2D-FES obtained from the dehydration reactions of *cv* and *tv* smectites at 700 K (Online Materials[1] Fig. S9a), together with its projection onto CV1, are depicted in Figure 5. The free energy barriers of *cv* and *tv* smectites were estimated to be 14.2 and 10.3 kcal/mol at 700 K, respectively. The results demonstrated that the *cv* smectite exhibits a higher dehydration energy barrier than *tv* smectite at 700 K. At 900 K, the free energy barriers of *cv* and *tv* smectites were observed to be 7.4 and 9.5 kcal/mol, respectively (Fig. 5). Therefore, similar to the deprotonation step, the dehydration step is more sensitive to the temperature in the *cv* structure. With increasing temperature, the free energy barrier gets lower for *cv* than *tv*.

**Dehydroxylation mechanism.** The thermal reaction energy barriers for the deprotonation and intralayer dehydration steps and the total energy barriers are summarized in Figure 6.

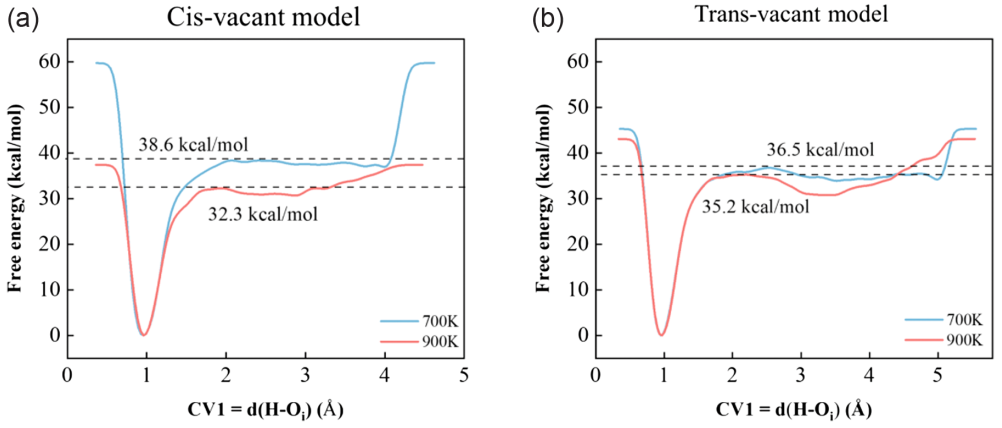


**Figure 4.** The FES projection on CV1 for the deprotonation reaction simulations of *cv* (**a**) and *tv* (**b**) smectites with *cross* mechanism at 700 and 900 K. (Color online.)

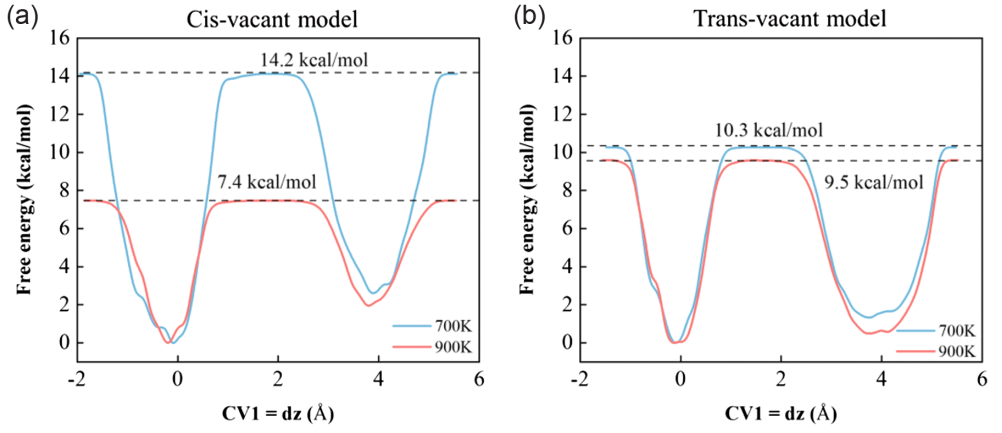


**Figure 5.** The FES projection on CV1 for the intralayer dehydration reaction simulations of *cv* (**a**) and *tv* (**b**) smectites at 700 and 900 K (Color online.)

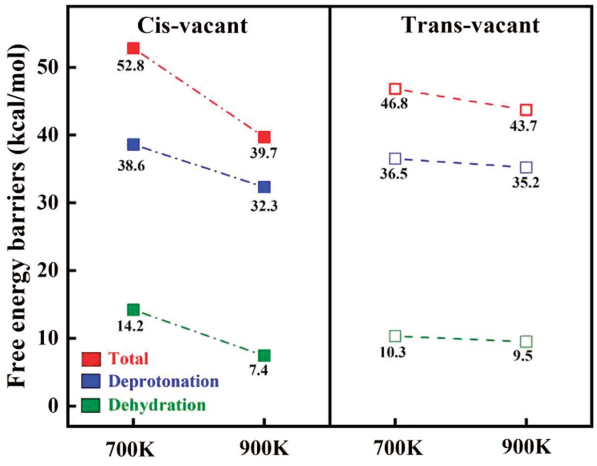


**Figure 6.** Free energy barriers (in kcal/mol) of thermal reactions for *cv* and *tv* smectites. (Color online.)

The total energy barrier for the *cv* smectite at 700 K was higher by 6 kcal/mol than that of the *tv* (i.e., 52.8 vs. 46.8 kcal/mol), indicating that dehydroxylation is more difficult for the *cv* smectite than the *tv* at this temperature. However, as the temperature increases to 900 K, the total energy barrier of the *cv* smectite decreased significantly, even lower than that of *tv* smectite (i.e., 39.7 vs. 43.7 kcal/mol), which means that the thermal dehydroxylation reaction becomes relatively feasible for the *cv*. As we see, the dehydroxylation reaction of *cv* smectite demonstrated more sensitivity to elevated temperature, suggesting that as the temperature increased from 700 to 900 K, the dehydroxylation reaction of *cv* smectite gets similar to that of *tv* smectite. This finding provides a mechanistic basis for the observed different dehydroxylation temperature ranges for *cv* and *tv* smectites in TGA analysis (Derkowski and Kuligiewicz 2022).

To reveal the structures of the dehydroxylation products, we performed equilibrium ReaxFF molecular dynamics on dehydroxylated *cv* and *tv* smectites (for the initial see Online Materials[1] Fig. S3). Figure 7 illustrated the snapshots of the *cv* and *tv* models at 700 K derived at different simulation times. We carried out an analysis of the structures derived from the simulation trajectories. The initial structures (i.e., 0 ps) of *cv* and *tv* dehydroxylated smectites are shown in Figure 7a. The aluminum sheet consists of unstable five-coordinated aluminum sites, characterized as quadrangular-pyramids, where each site is surrounded by four central O atoms and one bridging O atom ($O_b$) (Fig. 7a). It is worth noting that in *tv* models, the bridging O atom serves as a single bridge connecting two aluminum atoms, whereas, in *cv* dehydroxylation models, the bridging O atom and one central O atom simultaneously connect two aluminum atoms (Fig. 7a), implying that the structural transformation is more complicated in the *cv* dehydroxylated model than in the *tv* dehydroxylated model.

As structural transformations occur (150 ps), the layer structure of the *cv* model was significantly distorted (Fig. 7b). However, only a slight distortion was observed in the silicate tetrahedra of the *tv* smectite during the process, and the Al quadrangular-pyramid was easily transformed into Al trigonal-bipyramids through the single bridging O atom movement only (Fig. 7b). Consequently, elevated temperature can overcome the structural transformation barrier of *cv* smectite, thereby significantly reducing the thermal reaction barrier (39.7 kcal/mol at 900 K and 52.8 kcal/mol at 700 K, respectively), while it is not obvious for *tv* smectite.

At 300 ps, the dehydroxylated structure of *cv* and *tv* smectites no longer changes significantly and are found to be identical (Fig. 7c). In this structure, the initial five-coordinated aluminum sites (quadrangular-pyramid) in both models (Fig. 7a) transformed into five-coordinated aluminum sites (trigonal-bipyramids) (Fig. 7c). Meanwhile, the structure found was also consistent with

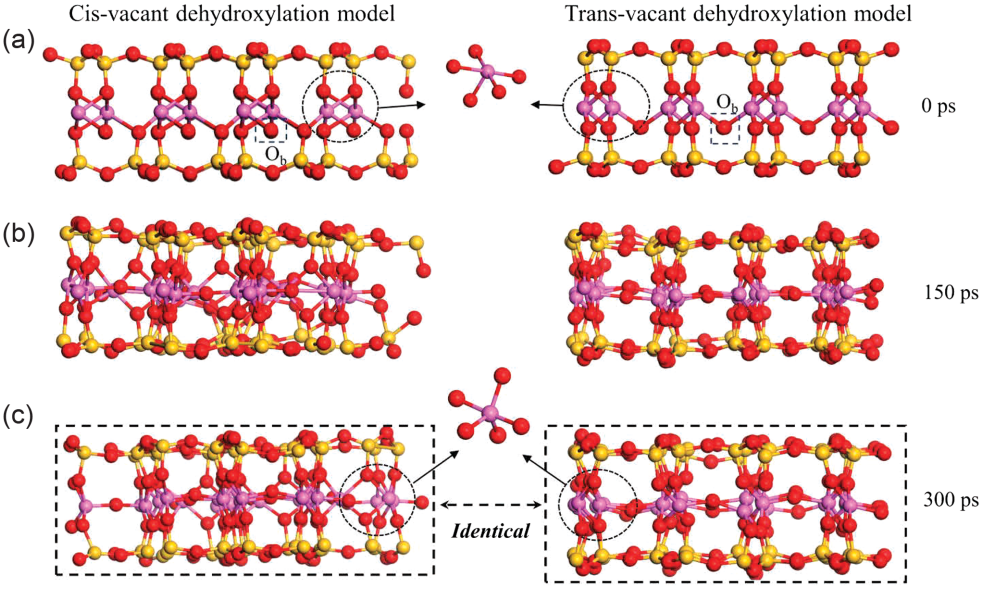


**Figure 7.** Snapshots of *cv* and *tv* smectites dehydration models at 700 K for 0 ps (**a**), 150 ps (**b**), and 300 ps (**c**). (Color online.)

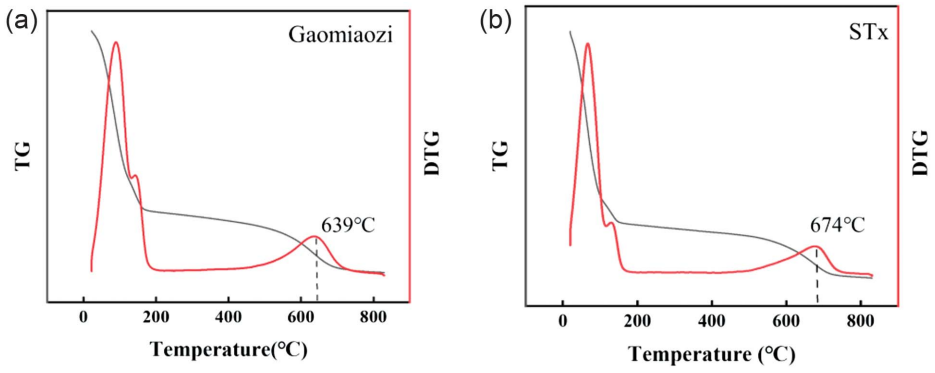


**Figure 8.** DTA curves of Gaomiaozi- (**a**) and Stx-smectite (**b**). (Color online.)

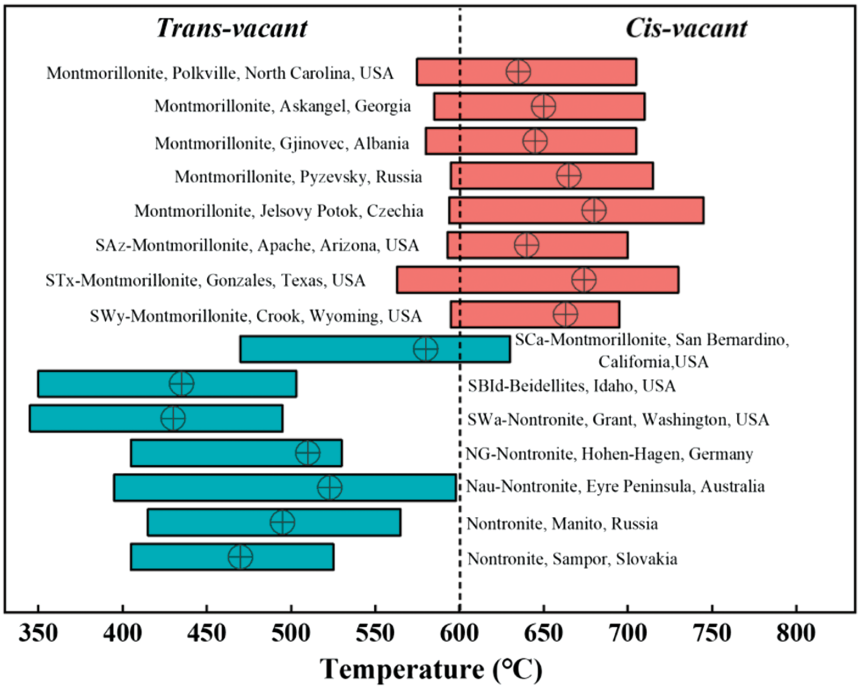


**Figure 9.** Dehydroxylation temperatures range and peak values of DTA and *cv*/*tv* types of smectites from various regions in Europe and the U.S.A. (Color online.)

previous simulation studies of the *tv* smectite dehydroxylated model (Guggenheim et al. 1987; Molina-Montes et al. 2010; Muñoz-Santiburcio et al. 2012), which deserves experimental verification in the future.

### Thermogravimetric analysis and China smectite types

The molecular simulation results elucidated the mechanisms by which the dehydroxylation temperature boundary can be employed to determine the *cv*/*tv* type. Hence, we collected representative smectite samples from China (Gaomiaozi) and the U.S.A. (Stx) and conducted TGA to elucidate the structural types (Fig. 8). The dehydroxylation temperatures determined by differential thermal analysis (DTA) were found to be 639 and 674 °C for Gaomiaozi- and Stx-smectites, respectively. The results indicated that the Gaomiaozi-smectite in China and STx-smectite in the U.S.A. exhibited characteristics of *cv* structure. Together with previous studies (El-Barawy et al. 1986; Ding and Frost 2002; Wolters and Emmerich 2007; Che et al. 2011; Skoubris et al. 2013; Derkowski and Kuligiewicz 2022; Plevová and Vaculíková 2024), STx-, SAz-, and SWy-smectites (montmorillonite) were found to be the *cv* structures, while SCa-smectite (montmorillonite), SWa-, Nau-, NG-smectites (nontronite), and SBId-smectite (beidellite) were *tv* structures. It can also be seen that most montmorillonite samples predominantly exhibit *cv* structure, whereas nontronite and beidellite primarily exhibit *tv* structure in Europe and the U.S.A. (Fig. 9).

Based on a comprehensive review of existing literature, we summarized the dehydroxylation temperatures from TGA for smectite samples sourced from various regions across China (Fig. 10) (Wu et al. 1999; Hou et al. 2003; Qin et al. 2021). The samples are from 10 provinces in China and are the most representative smectites in China. As we see, the smectites from most regions in China exhibit *cv* structures, which is consistent with previous findings reported in other geographical areas (Subramanian et al. 2020; Orucoglu et al. 2022). The peak value of the Santai sample is near 600 °C, and the

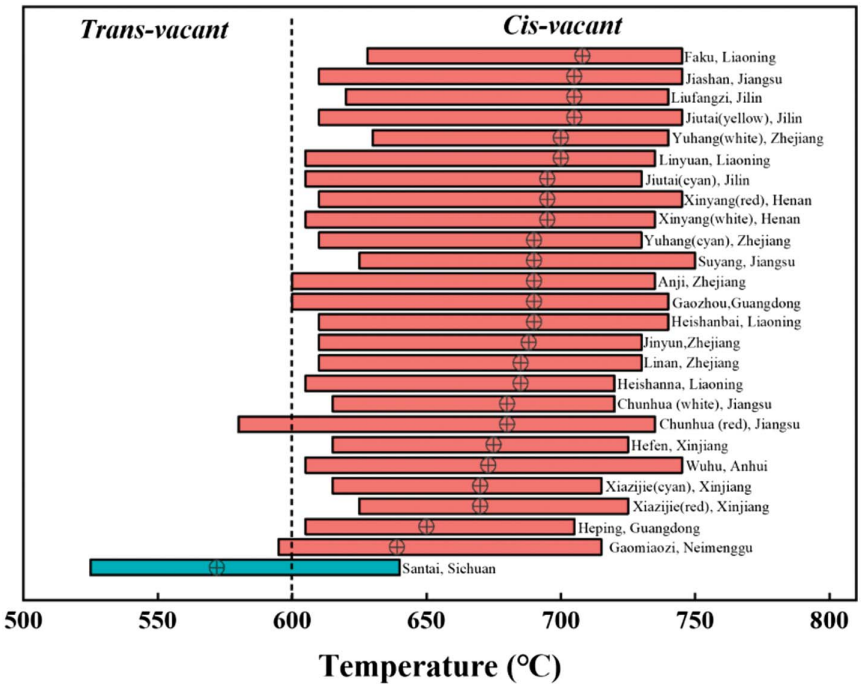


**Figure 10.** Dehydroxylation temperatures range and peak values of DTA and *cv*/*tv* types of smectites from various regions in China. Wuhu and Santai smectites' peak values were derived from TG curves (Qin et al. 2021). (Color online.)

temperature range is 525–640 °C, implying that it consists of both structures. In particular, Gaomiaozi smectite is suggested as a candidate backfill material for China's nuclear waste repository (Chen et al. 2014). Therefore, future research on the properties of its buffering performance, such as adsorption and swelling properties, should focus on the *cv* model. Molecular-level modeling studies on the *cv* are in urgent need, considering that most of the previous molecular simulation studies were based on the *tv*.

## Implications

Our ReaxFF molecular dynamics simulation results elucidated the thermal reaction mechanism and high-temperature transformation of *cis*-vacant (*cv*) and *trans*-vacant (*tv*) smectites at the atomic level. The findings provide a theoretical basis for the application of the dehydroxylation temperature boundary method in determining smectite type. We summarized the dehydroxylation temperatures of smectite samples from China, U.S.A., and Europe. Classification results suggested that montmorillonites predominantly exhibit *cv* structure, whereas nontronite and beidellite are primarily *tv* structures. Furthermore, almost all smectites from China exhibit *cv* structures. At the most fundamental level, our study reveals the thermal behavior difference between *cv* and *tv* smectites, further emphasizing the necessity that the investigation of natural smectite properties should be grounded in realistic models. Overall, this work serves as a basis for future applications of smectites in various fields.

## Acknowledgments and Funding

This study was supported by the National Natural Science Foundation of China (Grant Nos. 42125202, 42402043, 42421002, and 42302038), Postdoctoral Fellowship Program of CPSF (Grant No. GZC20240674), China Postdoctoral Science Foundation (Grant No. 2022M721547), and Jiangsu Funding Program for Excellent Postdoctoral Talent (Grant No. 2023ZB411). We appreciate the help from Hongjuan Sun. We acknowledge the financial support from the State Key Laboratory for Mineral Deposits Research at Nanjing University. We are grateful to the High Performance Computing Center (HPCC) of Nanjing University for doing the numerical calculations in this paper on its blade cluster system.

## References Cited

Aktulga, H.M., Fogarty, J.C., Pandit, S.A., and Grama, A.Y. (2012) Parallel reactive molecular dynamics: Numerical methods and algorithmic techniques. Parallel Computing, 38, 245–259, https://doi.org/10.1016/j.parco.2011.08.005.

Bergaya, F. and Lagaly, G. (2006) Chapter 1: General introduction: Clays, clay minerals, and clay science. In F. Bergaya, B.K.G. Theng, and G. Lagaly, Eds., Developments in Clay Science Vol. 1, p. 1–18. Elsevier.

Brigatti, M.F., Galan, E., and Theng, B.K.G. (2006) Chapter 2: Structures and mineralogy of clay minerals. In F. Bergaya, B.K.G. Theng, and G. Lagaly, Eds., Developments in Clay Science Vol. 1, p. 19–86. Elsevier.

Che, C., Glotch, T.D., Bish, D.L., Michalski, J.R., and Xu, W. (2011) Spectroscopic study of the dehydration and/or dehydroxylation of phyllosilicate and zeolite minerals. Journal of Geophysical Research, 116, 0148–0227.

Chen, L., Liu, Y., Wang, J., Cao, S., Xie, J., Ma, L., Zhao, X., Li, Y., and Liu, J. (2014) Investigation of the thermal-hydro-mechanical (THM) behavior of GMZ bentonite in the China-Mock-up test. Engineering Geology, 172, 57–68, https://doi.org/10.1016/j.enggeo.2014.01.008.

Cygan, R.T., Greathouse, J.A., and Kalinichev, A.G. (2021) Advances in Clayff molecular simulation of layered and nanoporous materials and their aqueous interfaces. The Journal of Physical Chemistry C, 125, 17573–17589, https://doi.org/10.1021/acs.jpcc.1c04600.

Derkowski, A. and Kuligiewicz, A. (2022) Thermal analysis and thermal reactions of smectites: A review of methodology, mechanisms, and kinetics. Clays and Clay Minerals, 70, 946–972, https://doi.org/10.1007/s42860-023-00222-y.

Derkowski, A., Drits, V.A., and McCarty, D.K. (2012) Nature of rehydroxylation in dioctahedral 2:1 layer clay minerals. American Mineralogist, 97, 610–629, https://doi.org/10.2138/am.2012.3871.

Ding, Z. and Frost, R.L. (2002) Controlled rate thermal analysis of nontronite. Thermochimica Acta, 389, 185–193, https://doi.org/10.1016/S0040-6031(02)00059-X.

Drits, V.A., Besson, G., and Muller, F. (1995) An improved model for structural transformations of heat-treated aluminous dioctahedral 2:1 layer silicates. Clays and Clay Minerals, 43, 718–731, https://doi.org/10.1346/CCMN.1995.0430608.

El-Barawy, K.A., Girgis, B.S., and Felix, N.S. (1986) Thermal treatment of some pure smectites. Thermochimica Acta, 98, 181–189, https://doi.org/10.1016/0040-6031(86)87088-5.

Emmerich, K., Wolters, F., Kahr, G., and Lagaly, G. (2009) Clay profiling: The classification of montmorillonites. Clays and Clay Minerals, 57, 104–114, https://doi.org/10.1346/CCMN.2009.0570110.

Fitzgerald, J.J., Hamza, A.I., Dec, S.F., and Bronnimann, C.E. (1996) Solid-state $^{27}$Al and $^{29}$Si NMR and $^{1}$H CRAMPS Studies of the thermal transformations of the 2:1 phyllosilicate pyrophyllite. Journal of Physical Chemistry, 100, 17351–17360, https://doi.org/10.1021/jp961499f.

Frenkel, D. and Smit, B. (2002) Introduction. In D. Frenkel and B. Smit, Eds., Understanding Molecular Simulation, 2nd ed., p. 1–6. Academic Press.

Gao, P., Liu, X., Guo, Z., and Tournassat, C. (2023) Acid-base properties of *cis*-vacant montmorillonite edge surfaces: A combined first-principles molecular dynamics and surface complexation modeling approach. Environmental Science & Technology, 57, 1342–1352, https://doi.org/10.1021/acs.est.2c07171.

——— (2024) Influence of Fe(II), Fe(III), and Al(III) isomorphic substitutions on acid-base properties of edge surfaces of *cis*-vacant montmorillonite: Insights from first-principles molecular dynamics simulations and surface complexation modeling. American Mineralogist, 109, 1162–1170, https://doi.org/10.2138/am-2023-9057.

Geiger, C. (2008) Silicate garnet: A micro to macroscopic (re)view. American Mineralogist, 93, 360–372, https://doi.org/10.2138/am.2008.2588.

Guggenheim, S., Chang, Y.-H., and Koster van Gross, A.F. (1987) Muscovite dihydroxylation: High-temperature studies. American Mineralogist, 72, 537–550.

Guimarães, V. and Bobos, I. (2021) Role of clay barrier systems in the disposal of radioactive waste. In A. Núñez-Delgado, Ed., Sorbents Materials for Controlling Environmental Pollution. Chapter 20, 513–541. Elsevier.

Heinz, H., Lin, T.-J., Kishore Mishra, R., and Emami, F.S. (2013) Thermodynamically consistent force fields for the assembly of inorganic, organic, and biological nanostructures: The INTERFACE force field. Langmuir, 29, 1754–1765, https://doi.org/10.1021/la3038846.

Heller-Kallai, L. (2013) Thermally modified clay minerals. In F. Bergaya and G. Lagaly, Eds., Developments in Clay Science, Vol. 5, p. 411–433. Elsevier.

Hou, M., Xia, Z., Gao, Y., Ma, B., Wan, H., and Ma, Y. (2003) Thermal properties of various bentonites. Rock and Mineral Analysis, 263–268 (in Chinese).

Koster van Gross, A.F. and Guggenheum, S. (1989) Dehydroxylation of Ca- and Mg-exchanged montmorillonite. American Mineralogist, 74, 627–636.

Laio, A. and Parrinello, M. (2002) Escaping free-energy minima. Proceedings of the National Academy of Sciences of the United States of America, 99, 12562–12566, https://doi.org/10.1073/pnas.202427399.

Lantenois, S., Muller, F., Bény, J.-M., Mahiaoui, J., and Champallier, R. (2008) Hydrothermal synthesis of beidellites: Characterization and study of the *cis*- and *trans*-vacant character. Clays and Clay Minerals, 56, 39–48, https://doi.org/10.1346/CCMN.2008.0560104.

Manceau, A., Lanson, B., Drits, V.A., Chateigner, D., Gates, W.P., Wu, J., Huo, D., and Stucki, J.W. (2000) Oxidation-reduction mechanism of iron in dioctahedral smectites: 1. Crystal chemistry of oxidized reference nontronites. American Mineralogist, 85, 133–152, https://doi.org/10.2138/am-2000-0114.

Martyna, G.J., Klein, M.L., and Tuckerman, M. (1992) Nosé-Hoover chains: The canonical ensemble via continuous dynamics. The Journal of Chemical Physics, 97, 2635–2643, https://doi.org/10.1063/1.463940.

Molina-Montes, E., Timón, V., Hernández-Laguna, A., and Sainz-Díaz, C.I. (2008a) Dehydroxylation mechanisms in $Al^{3+}/Fe^{3+}$ dioctahedral phyllosilicates by quantum mechanical methods with cluster models. Geochimica et Cosmochimica Acta, 72, 3929–3938, https://doi.org/10.1016/j.gca.2008.04.043.

Molina-Montes, E., Donadio, D., Hernández-Laguna, A., Sainz-Díaz, C.I., and Parrinello, M. (2008b) DFT research on the dehydroxylation reaction of pyrophyllite 1. First-principle molecular dynamics simulations. The Journal of Physical Chemistry B, 112, 7051–7060, https://doi.org/10.1021/jp711278s.

Molina-Montes, E., Donadio, D., Hernández-Laguna, A., and Sainz-Díaz, C.I. (2008c) DFT research on the dehydroxylation reaction of pyrophyllite 2. Characterization of reactants, intermediates, and transition states along the reaction path. The Journal of Physical Chemistry A, 112, 6373–6383, https://doi.org/10.1021/jp8010876.

——— (2010) Exploring the rehydroxylation reaction of pyrophyllite by ab initio molecular dynamics. The Journal of Physical Chemistry B, 114, 7593–7601, https://doi.org/10.1021/jp102239k.

Molina-Montes, E., Donadio, D., Hernández-Laguna, A., Parrinello, M., and Sainz-Díaz, C.I. (2013) Water release from pyrophyllite during the dehydroxylation process explored by quantum mechanical simulations. The Journal of Physical Chemistry C, 117, 7526–7532, https://doi.org/10.1021/jp310739y.

Muñoz-Santiburcio, D., Kosa, M., Hernández-Laguna, A., Sainz-Díaz, C.I., and Parrinello, M. (2012) Ab initio molecular dynamics study of the dehydroxylation reaction in a smectite model. The Journal of Physical Chemistry C, 116, 12203–12211, https://doi.org/10.1021/jp301366r.

Muñoz-Santiburcio, D., Hernández-Laguna, A., and Sainz-Díaz, C.I. (2016) Simulating the dehydroxylation reaction in smectite models by Car-Parrinello-Like-Born-Oppenheimer molecular dynamics and metadynamics. The Journal of Physical Chemistry C, 120, 28186–28192, https://doi.org/10.1021/acs.jpcc.6b10436.

Orucoglu, E., Grangeon, S., Gloter, A., Robinet, J.-C., Madé, B., and Tournassat, C. (2022) Competitive adsorption processes at clay mineral surfaces: A coupled experimental and modeling approach. ACS Earth & Space Chemistry, 6, 144–159, https://doi.org/10.1021/acsearthspacechem.1c00323.

Plevová, E. and Vaculíková, L. (2024) Thermal behavior of ceramic bodies based on fly ash and smectites. Minerals, 14, 334, https://doi.org/10.3390/min14040334.

Plimpton, S. (1995) Fast parallel algorithms for short-range molecular dynamics. Journal of Computational Physics, 117, 1–19, https://doi.org/10.1006/jcph.1995.1039.

Qin, Y., Peng, T., Sun, H., Zhou, C., and Chao, L. (2021) The effect of high temperature treatment on the structure of sodium bentonite montmorillonite. Sichuan Daxue Xuebao. Ziran Kexue Ban, 58, 035002 (in Chinese).

Senftle, T.P., Hong, S., Islam, M.M., Kylasa, S.B., Zheng, Y., Shin, Y.K., Junkermeier, C., Engel-Herbert, R., Janik, M.J., Aktulga, H.M., and others. (2016) The ReaxFF reactive force-field: Development, applications and future directions. npj Computational Materials, 2, 15011.

Skoubris, E.N., Chryssikos, G.D., Christidis, G.E., and Gionis, V. (2013) Structural characterization of reduced-charge montmorillonites. Evidence based on FTIR spectroscopy, thermal behavior, and layer-charge systematics. Clays and Clay Minerals, 61, 83–97, https://doi.org/10.1346/CCMN.2013.0610207.

Stackhouse, S., Coveney, P.V., and Benoit, D.M. (2004) Density-functional-theory-based study of the dehydroxylation behavior of aluminous dioctahedral 2:1 layer-type clay minerals. The Journal of Physical Chemistry B, 108, 9685–9694, https://doi.org/10.1021/jp037608p.

Subramanian, N., Whittaker, M.L., Ophus, C., and Lammers, L.N. (2020) Structural implications of interfacial hydrogen bonding in hydrated Wyoming-montmorillonite clay. The Journal of Physical Chemistry C, 124, 8697–8705, https://doi.org/10.1021/acs.jpcc.9b11339.

Tong, Y., Zhang, H., Li, X., and Jia, Q. (2023) Experimental study on sodium modification and purification of GMZ bentonite. Construction & Building Materials, 367, 130060, https://doi.org/10.1016/j.conbuildmat.2022.130060.

Tournassat, C., Steefel, C.I., Bourg, I.C., and Bergaya, F., Eds. (2015) Natural and Engineered Clay Barriers, 446 p. Elsevier.

Tribello, G.A., Bonomi, M., Branduardi, D., Camilloni, C., and Bussi, G. (2014) PLUMED 2: New feathers for an old bird. Computer Physics Communications, 185, 604–613, https://doi.org/10.1016/j.cpc.2013.09.018.

Tsipursky, S.I. and Drits, V.A. (1984) The distribution of octahedral cations in the 2:1 layers of dioctahedral smectites studied by oblique-texture electron diffraction. Clay Minerals, 19, 177–193, https://doi.org/10.1180/claymin.1984.019.2.05.

van Duin, A.C.T., Dasgupta, S., Lorant, F., and Goddard, W.A. (2001) ReaxFF: A reactive force field for hydrocarbons. The Journal of Physical Chemistry A, 105, 9396–9409, https://doi.org/10.1021/jp004368u.

Vantelon, D., Pelletier, M., Michot, L.J., Barres, O., and Thomas, F. (2001) Fe, Mg and Al distribution in the octahedral sheet of montmorillonites. An infrared study in the OH-bending region. Clay Minerals, 36, 369–379, https://doi.org/10.1180/000985501750539463.

Wang, L., Zhang, M., Redfern, S.A.T., and Zhang, Z. (2002) Dehydroxylation and transformations of the 2:1 phyllosilicate pyrophyllite at elevated temperatures: An infrared spectroscopic study. Clays and Clay Minerals, 50, 272–283, https://doi.org/10.1346/000986002760832874.

Wolters, F. and Emmerich, K. (2007) Thermal reactions of smectites—Relation of dehydroxylation temperature to octahedral structure. Thermochimica Acta, 462, 80–88, https://doi.org/10.1016/j.tca.2007.06.002.

Worasith, N. and Goodman, B.A. (2023) Clay mineral products for improving environmental quality. Applied Clay Science, 242, 106980, https://doi.org/10.1016/j.clay.2023.106980.

Wu, P., Zhang, H., Guo, J., Hu, C., and Liu, X. (1999) MAS NMR spectra of montmorillonite and its thermal treatment products. Journal of Inorganic Materials, 14, 580–586 (in Chinese).

Zhang, Y., Liu, X., van Duin, A.C.T., Lu, X., and Meijer, E.J. (2024) Development and validation of a general-purpose ReaxFF reactive force field for earth material modeling. The Journal of Chemical Physics, 160, 094103, https://doi.org/10.1063/5.0194486.

Manuscript received April 26, 2024
Manuscript accepted August 19, 2024
Accepted manuscript online August 27, 2024
Manuscript Handled by Mainak Mookherjee

## Endnotes:

[1]Deposit item AM-25-59445. Online Materials are free to all readers. Go online, via the table of contents or article view, and find the tab or link for supplemental materials.